Cellular Microbiology (2013) doi:10.1111/cmi.12144

The actin-based machinery of *Trichomonas vaginalis* mediates flagellate-amoeboid transition and migration across host tissue

Gary Kusdian, Christian Woehle, William F. Martin and Sven B. Gould*
Institute for Molecular Evolution, Heinrich-Heine-University Düsseldorf, 40225 Düsseldorf, Germany.

Summary

***Trichomonas vaginalis* is the most widespread non-viral pathogen of the human urogenital tract, infecting ~ 3% of the world's population annually. At the onset of infection the protist changes morphology within minutes: the flagellated free-swimming cell converts into the amoeboid-adherent stage. The molecular machinery of this process is not well studied, but is thought to involve actin reorganization. We have characterized amoeboid transition, focusing in particular on *Tv*Fim1, the only expressed protein of the fimbrin family in *Trichomonas*. Addition of *Tv*Fim1 to actin polymerization assays increases the speed of actin filament assembly and results in bundling of F-actin in a parallel and anti-parallel manner. Upon contact with vaginal epithelial cells, the otherwise diffuse localization of actin and *Tv*Fim1 changes dramatically. In the amoeboid *Tv*Fim1 associates with fibrous actin bundles and concentrates at protrusive structures opposing the trailing ends of the gliding amoeboid form and rapidly redistributes together with actin to form distinct clusters. Live cell imaging demonstrates that *Trichomonas* amoeboid stages do not just adhere to host tissue, rather they actively migrate across human epithelial cells. They do so in a concerted manner, with an average speed of 20 μm min^{-1} and often using their flagella and apical tip as the leading edge.**

Introduction

Trichomonas vaginalis is the most widespread non-viral and sexually transmitted human parasite worldwide (Benchimol, 2004). Its genome encodes approximately 60 000 proteins, at least twice as many as its mammalian host (Carlton *et al*., 2007). Of the many hundred million *T. vaginalis* infections that occur annually, the majority is asymptomatic, while a minority results in trichomoniasis with urogenital tract swelling and inflammatory discharge. However, asymptomatic infections decrease fertility, increase the risk of acquiring HIV and elevate the risk of prostate and cervical cancer (Petrin *et al*., 1998; Stark *et al*., 2009; Ryan *et al*., 2011). Trichomoniasis is commonly treated with nitroimidazole derivates, but resistant strains are on the rise (Kulda, 1999; Upcroft and Upcroft, 2001; Benchimol, 2008).

As an essential component of *T. vaginalis* urogenital tract colonization, minutes after contact with human urogenital tract cells, *T. vaginalis* undergoes a radical change in cell morphology (Lal *et al*., 2006). The free-swimming flagellate cell flattens and spreads out over the host cell tissue to become an amoeba. This ability to shift from a flagellate-motile to an adherent-amoeboid cell stage is rare among protists and, outside the trichomonads, only known among a few species such as *Naegleria gruberi* and *Physarum polycephalum* (Fritz-Laylin *et al*., 2010a; Ryan *et al*., 2011). With only a few minutes to complete, this amoeboid transition is the fastest described and far more rapid than the *N. gruberi* transformation, which can require more than an hour (Fulton, 1993; Fritz-Laylin *et al*., 2010b).

Little is known about the molecular machinery behind amoeboid transition, how it is orchestrated or the components involved. Clues come however from the circumstance that the amoeboid transition connects the two types of cellular locomotion known among eukaryotes: tubulin-based flagellar swimming and actin-based amoeboid gliding. Actin and tubulin are the core components of these locomotion types and of the eukaryotic cytoskeleton in general. Although the proteins associated with these two types of locomotion are ubiquitous among eukaryotic genomes, few species exhibit both types during their life cycle (Fig. 1). In amoeba and apicomplexan parasites, the actin-based cytoskeleton is the key component of gliding locomotion (Fukui, 2002; Baum *et al*., 2008). The apicomplexan machinery is known as the glideosome and becomes active when the parasites need to overcome biological barriers or invade new host cells (Santos *et al*., 2009). Previous reports localized the actin-binding

Received 27 December, 2012; revised 16 March, 2013; accepted 20 March, 2013. *For correspondence. E-mail gould@hhu.de; Tel. (+49) 211 811 3983; Fax (+49) 211 811 3554.

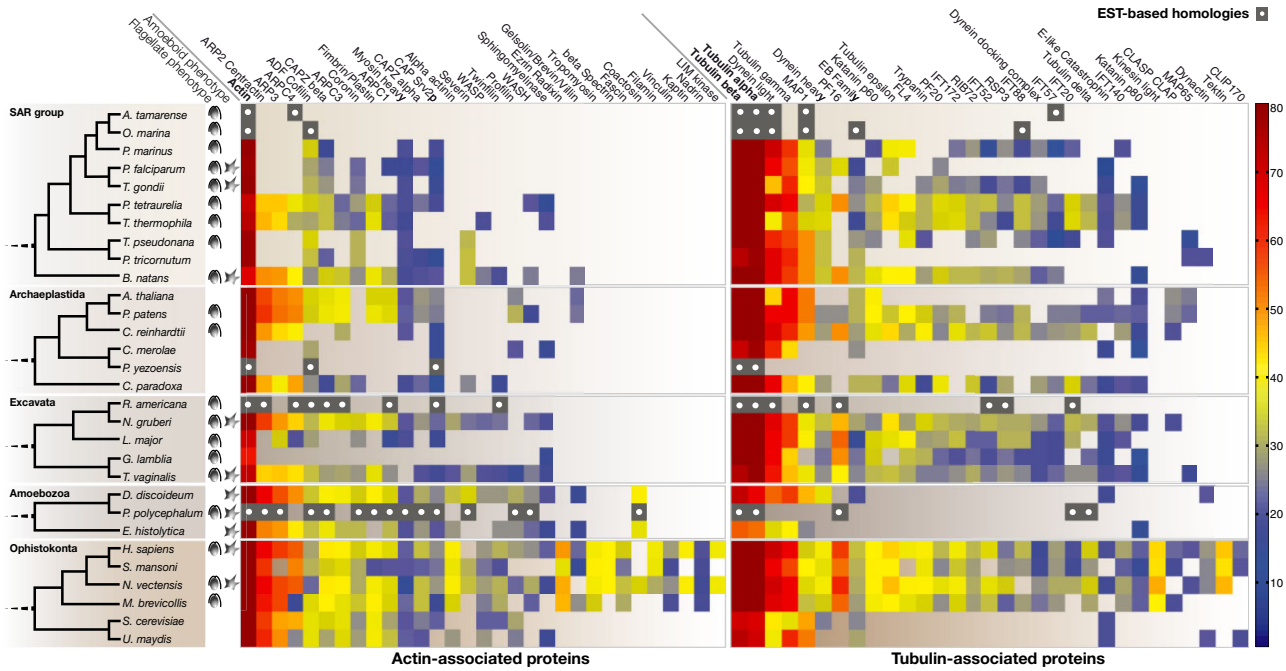

Fig. 1. Heat map of actin, tubulin and selected associated proteins. Clusters of orthologous genes (query sequences Table S1) are sorted by the sum of average similarity to all cluster members and represented by the heat map in percent. The cladogram on the left shows a schematic relationship within the five eukaryotic kingdoms and earlier branching is not shown due to its uncertainty. The SAR group unites *s*tramenopiles, *a*lveolates and *r*hizaria. Symbols indicate whether organisms of the individual groups display flagellate and/or amoeboid phenotypes (pyriform-shape and star-shape respectively).

proteins alpha-actinin and coronin to the periphery of *T. vaginalis* amoeboid cells, suggesting that parabasalian amoeboid transformation might involve rearrangement of the actin cytoskeleton (Brugerolle *et al.*, 1996; Addis *et al.*, 1998; Bricheux *et al.*, 1998; 2000) and actin polymerization blockers influence the ability of the parasite to adhere to plastic surfaces (Gold and Ofek, 1992).

In contrast to the intestinal parasite *Giardia intestinalis*, in which common eukaryotic acting regulators are absent (Paredez *et al.*, 2011), the *T. vaginalis* genome encodes a variety of standard actin-associated and regulating proteins (Fig. 1). The only putative actin-bundling proteins of *Trichomonas* appear to be alpha-actinins (up to five copies) and two proteins of the fimbrin family, also known as plastins (Aurrecoechea *et al.*, 2009; Elmendorf *et al.*, 2010). These two actin-bundling families contain calponin homology (CH) domains in tandem – each pair making up one actin binding domain (ABD) – and additional Ca^{++} binding EF-hands (Korenbaum and Rivero, 2002). But in contrast to alpha-actinin, in which the EF-hands are usually located at the C-terminus of the protein and separated from the ABDs by a coiled-coil region, the EF-hand in fimbrin occurs N-terminal, directly adjacent to the ABDs (Korenbaum and Rivero, 2002). For human and *Dictyostelium* fimbrin it has been shown that binding of Ca^{++} to the EF-hand blocks the protein's ability to bind to filamentous actin (Namba *et al.*, 1992; Prassler *et al.*, 1997). Only one of the two putative fimbrin proteins of *T. vaginalis* harbours the N-terminal EF-hand and only for that one, *Tv*Fim1, expression evidence exists at TrichDB (Aurrecoechea *et al.*, 2009).

To address the question put forward in the original genome paper of *T. vaginalis*, whether the structural remodelling of amoeboid parasites really is actin-based (Carlton *et al.*, 2007), we characterized the localization shift of the actin cytoskeleton during infection. We focused on *Tv*Fim1, that we demonstrate to bundle actin filaments, and provide detailed evidence for the actin machinery not only to promote flagellate-amoeboid transition upon infection, but also to subsequently mediate active and concerted gliding across host tissue.

Results

Trichomonas *encodes the majority of canonical actin-associated proteins and only one functional fimbrin*

Based on human proteins associated with the actin and tubulin-based cytoskeleton, which are characterized and annotated the best, we screened for homologues among a range of eukaryotes with representatives from all major phylogenetic groups. *T. vaginalis* encodes the most canonical actin and tubulin cytoskeleton-associated proteins (Fig. 1). Among the actin-based cytoskeleton this

includes genes for capZ, cofilin, formin and the Arp2/3 complex, in addition to at least 29 genes (five orthologous groups) encoding proteins of the actin family itself. Overall, all actins share a 40% global sequence identity and expression evidence exists for almost all of them at TrichDB (Aurrecoechea *et al*., 2009). The major actin-bundling protein of filopodia, fascin (Jansen *et al*., 2011), appears absent from the *T. vaginalis* genome (Fig. 1). The parasite encodes two putative proteins of the fimbrin family; *Tv*Fim1 (TVAG_351310) and *Tv*Fim2 (TVAG_116370). Both contain two tandem actin-binding domains (ABDs), but only *Tv*Fim1 contains the N-terminal Ca^{++}-binding EF-hand, typical for proteins of the fimbrin/plastin family (Korenbaum and Rivero, 2002). Compared with *Tv*Fim1 and the human homologue *Hs*Fim1 (L-Plastin), *Tv*Fim2 appears to have experienced a 5′ truncation, which extends into the N-terminal region of the first CH domain (Fig. S1B). Overall, the two *Trichomonas* fimbrins share a sequence identity of 74%, which increases to 82% when considering only the region containing the two ABDs.

At TrichDB we identified 145 expressed sequence tags (ESTs) for *Tv*Fim1, but none for *Tv*Fim2, despite the ESTs originating from mRNA obtained under different conditions such as normal and low-glucose culture conditions or fibronectin-mediated cytoadherence. To confirm we performed reverse-transcriptase PCR on isolated RNA from exponentially growing cells of *T. vaginalis*, both flagellate and amoeboid stage, and were only able to demonstrate expression of *Tv*Fim1 (Fig. 2A). To determine whether the only expressed fimbrin gene is upregulated upon contact with host tissue we performed quantitative real-time PCR on RNA isolated from the free-swimming stage and at 5, 20 and 60 min after fibronectin induced morphogenesis. In two individual experiments, each using biological and technical triplicates, we observed no significant upregulation of *Tv*Fim1 over the first hour compared with the slightly upregulated 40S ribosomal protein S5 (Fig. 2B). Hence, the parasite expresses only its full-length fimbrin copy and this gene does not appear to experience a significant upregulation upon contact with host tissue.

Overall, *Tv*Fim1 shares a global sequence identity with the human homologue *Hs*Fim1 of 43%. An alignment of *Tv*Fim1 and its homologues from a range of eukaryotes shows that a high amount of conservation is found among the actin binding CH domains themselves (Fig. S1A). The amount of conservation of the individual amino acids thought to interact with actin (Klein *et al*., 2004; Galkin *et al*., 2008) is comparable to that of other fimbrins. Reconstructing the interaction of the actin-binding domains of *Tv*Fim1 with actin using the known crystal structure of the *Schizosaccharomyces pombe* fimbrin protein (PDB accession 1RT8) and the F-actin-fimbrin

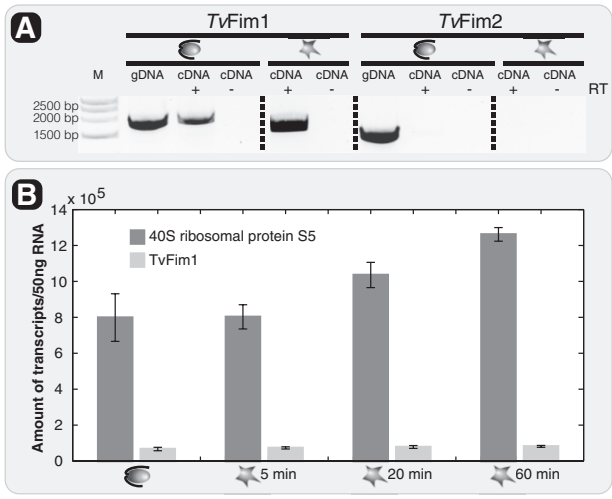

Fig. 2. A. Reverse transcriptase (RT) PCR on complementary DNA (cDNA) generated from motile and adherent cells (indicated by symbols as in Fig. 1) in the presence (+ RT) or, as control, absence of the reverse transcriptase enzyme (– RT), demonstrates the expression of *Tv*Fim1 only. Control PCR was performed on genomic DNA (gDNA).
B. Quantitative real-time PCR shows *Tv*Fim1 not to be significantly upregulated during infection compared with a copy of the ribosomal protein S5 (TVAG_158720).

ABD2 complex (PDB accession 3BYH), confirms the alignment sequence identity. The superposition of the two fimbrins of *S. pombe* and *T vaginalis* reveals no obvious difference and interacting residues within the CH3 and CH4 domain, such as E448, E523 or F602 (positions based on the alignment of Fig. S1A) are well conserved (Fig. 3).

Tv*Fim1 increases the actin polymerization rate and bundles F-actin*

Previous work on human and yeast fimbrins showed this protein family to bundle actin filaments (Namba *et al*., 1992; Prassler *et al*., 1997; Skau *et al*., 2011). To verify *Tv*Fim1's function as a fimbrin protein, and analyse the potential influence of *Tv*Fim1 on actin polymerization, we heterologously overexpressed a full-length C-terminally HIS-tagged version of *Tv*Fim1 in *Escherichia coli* and purified the protein using fast protein liquid chromatography (Fig. S2). All attempts to purify *T. vaginalis* actin failed to deliver sufficient quantities for *in vitro* studies, and we hence used actin purified from rabbit muscle and the amoeboid protist *Acanthamoeba* instead. We measured assembly kinetics of pyrene-labelled actin by fluorescence spectrophotometry and performed total internal reflection fluorescence microscopy (TIRF).

The pyrene assay showed that only *Acanthamoeba* actin polymerization significantly increased in the presence of *Tv*Fim1 and saturation of polymerization was

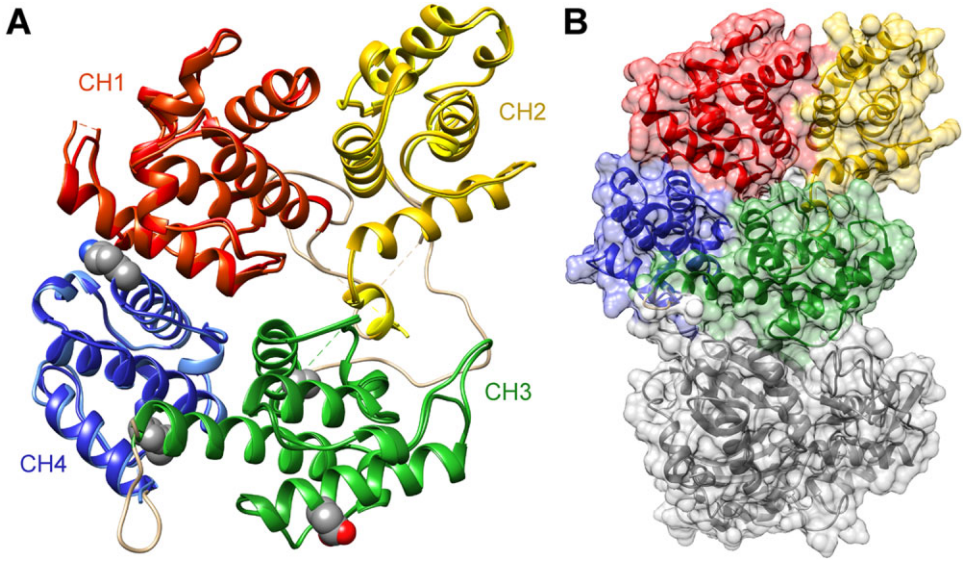

Fig. 3. Tertiary structure prediction of *Tv*Fim1.
A. Ribbon representation of the predicted tertiary conformation of *Tv*Fim1 (darker colours) superimposed onto the known crystal structure of the *S. pombe* fimbrin (lighter colours). Four exemplary amino acids that have been implicated to interact with F-actin are highlighted (grey, sphere representation) in the yeast sequence.
B. Semitransparent surface representation of *Tv*Fim1 (same colour code as in A) showing the interaction of the two CH domains 3 and 4 with an actin of *T. vaginalis* (grey; TVAG_337240). For details please refer to the text.

reached several minutes earlier (Fig. 4A). *Tv*Fim1 seems to stimulate the rate of *Acanthamoeba* actin assembly, but with no apparent polymerization effect on rabbit actin. However, TIRF imaging performed with rabbit actin demonstrated an intense parallel and anti-parallel bundling of actin filaments through *Tv*Fim1 (Fig. 4B). Dense bundles of many individual filaments were observed that continued to elongate at both ends of the bundles (Fig. 4C). We did not notice a favoured orientation of the aligned filaments, which is consistent with the bundling behaviour observed for yeast fimbrin (Skau *et al*., 2011).

Fimbrin and actin dynamics upon contact with host tissue

We generated a polyclonal peptide antibody directed against an epitope derived from the first ABD. The antibody detects a single band migrating below the 70 kDa marker lane, fitting well with the predicted mass of *Tv*Fim1 of approximately 68 kDa (Fig. S3A and B). Additionally we generated *Trichomonas* clones expressing haemagglutinin (HA) and green fluorescent protein (GFP)-tagged *Tv*Fim1 to further validate antibody specificity, avoid potential cross-talk of our fimbrin antibodies with the host cells and perform live imaging. In protein extract from cells expressing C-terminally HA-tagged *Tv*Fim1, a band migrating slightly slower compared with the endogenous copy – due to the HA-tag – was identified plus two faster migrating bands indicating putative proteolytic processing of the fusion protein (Fig. S3B).

In the free-swimming stage, *Tv*Fim1 localized to the cell periphery in a gradient-like manner and did not distinctly colocalize with actin (Fig. 5A–C). Identical localization was observed for the endogenously expressed protein, as well as for the HA-tagged copy, indicating that the C-terminal HA-tag did not influence the fusion-proteins localization (Fig. S3D). In adherent-amoeboid cells, which were induced through the exposure to a monolayer of vaginal epithelial cells (VECs), the observed localization pattern of *Tv*Fim1 changed dramatically. *Tv*Fim1 now begins to colocalize more specifically with actin, also in the still pyriform stage (Fig. 5E–G), but is predominantly observed to form clusters subtending the plasma membrane (Fig. 5M–O) and to associate with filamentous arrays (Figs 5I–K and S4E–G). We further observed filamentous structures (Figs 5I–K and S4E–G) similar to 'fibrous arrays' previously observed during the analyses of a coronin homologue in *Trichomonas* (Bricheux *et al*., 2000). Live imaging shows that the peripheral clusters at the migration front actually correspond to waves of fimbrin (Fig. 6). Specifically, at the contact sites clusters were observed and further around a contractile ring-like structure of a daughter cell budding from a multinuclear cell.

The time-lapse videos allowed to document different motion patterns of *T. vaginalis*, most importantly amoeboid migration across host tissue, only minutes upon

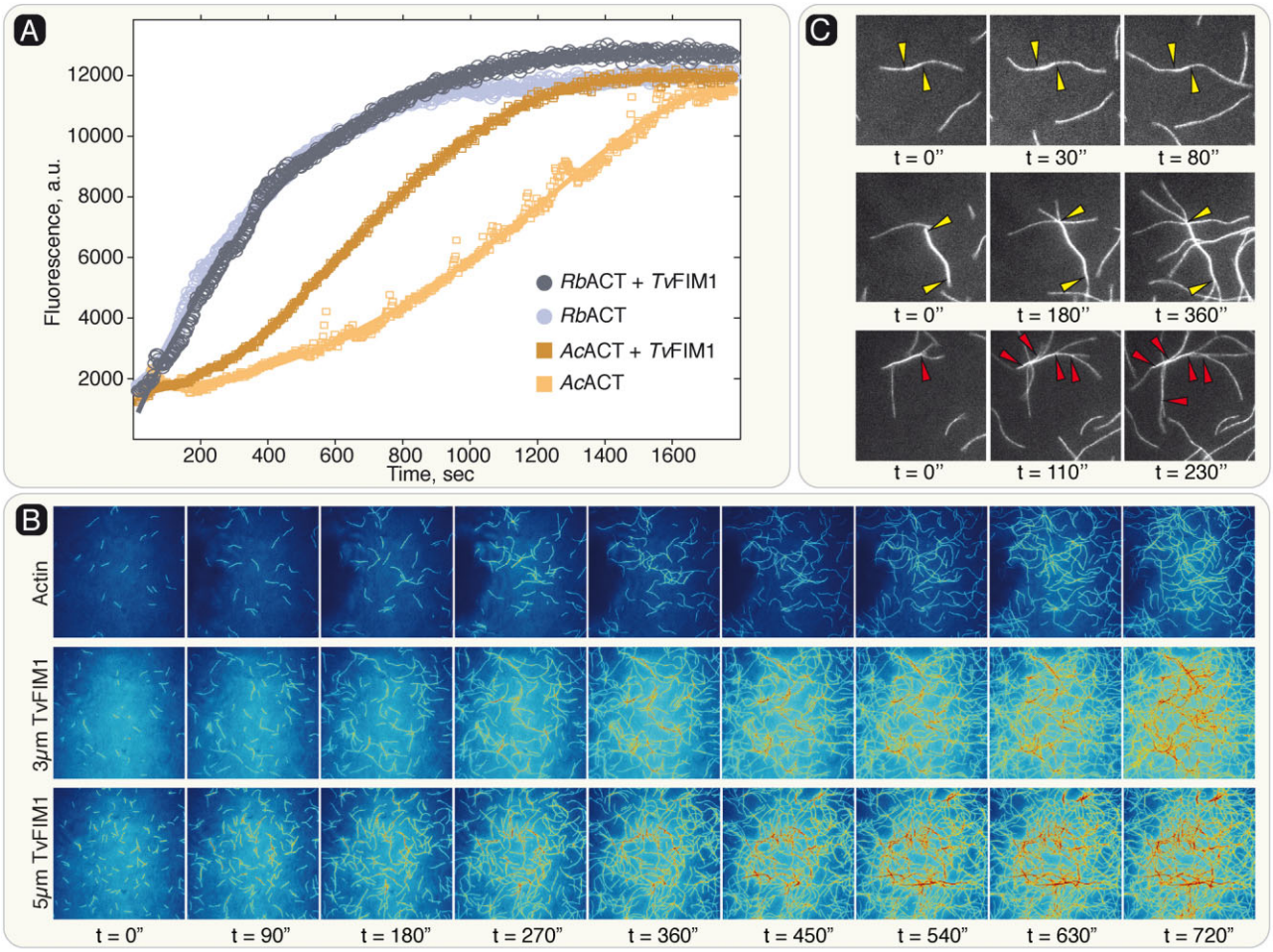

Fig. 4. Effect of *Tv*Fim1 on *in vitro* actin polymerization.
A. Polymerization assays of pyrene-labelled *Acantamoeba* (*Ac*ACT) and rabbit actin (*Rb*ACT) in the presence and absence of 4 μM *Tv*Fim1. Whereas no noticeable difference was observed for the polymerization rate of rabbit actin, the polymerization rate of the protozoan *Acantamoeba* actin was increased.
B. Rabbit muscle actin polymerization was monitored in the absence (Actin) and presence (3 and 5 μM) of purified *Tv*Fim1 using total internal reflection fluorescence microscopy and revealed a higher polymerization rate, as well as a strong parallel and anti-parallel bundling of actin filaments (see also Movies S2 and S3).
C. Details of F-actin bundled by *Tv*Fim1. Parallel and anti-parallel bundling is revealed by bundled filaments continuing to polymerize on both ends, marked by yellow arrow heads and at many branching points, marked by red arrow heads.

exposure to VECs (Movies S7–S10). *T. vaginalis* actively roams across the VEC-monolayer with an average speed of 20.2 μm min^{-1} (Table S3) and appears to use its flagella and apical tip as the guiding end (Fig. S5), which also appears to downright penetrate areas of adjacent and adherent VECs. One hour post infection we observed some amoeboid cells to massively increase their cell mass and adherent surface (Fig. S5); a process we refer to as juggernauting. The cells display multiple flagella pockets and nuclei (Figs S5 and S4K), which is consistent with previous observations (Yusof and Kumar, 2011). We observed individual *T. vaginalis* cells rapidly budding off from multinuclear cells, similar to what was described for *Tritrichomonas foetus* (Pereira-Neves and Benchimol, 2009). Overall, the cells appear highly agile while they migrate and scavenge from host tissue.

To determine whether the association of fimbrin and actin is specific for phenotypic plasticity induced through VECs, we investigated what happens during phagocytosis of *Saccharomyces*. Exponentially growing parasites were exposed to yeast cells in a 1:50 parasite/yeast ratio and incubated for 60 min in the CO_2 incubator – to be comparable to the other experiment – before fixation. We observed *T. vaginalis* to incorporate entire and multiple yeast cells at the same time, as previously documented (Pereira-Neves and Benchimol, 2007). As for the amoeboid form of the parasite, fimbrin now clearly colocalizes with actin, forming distinct rings around the large

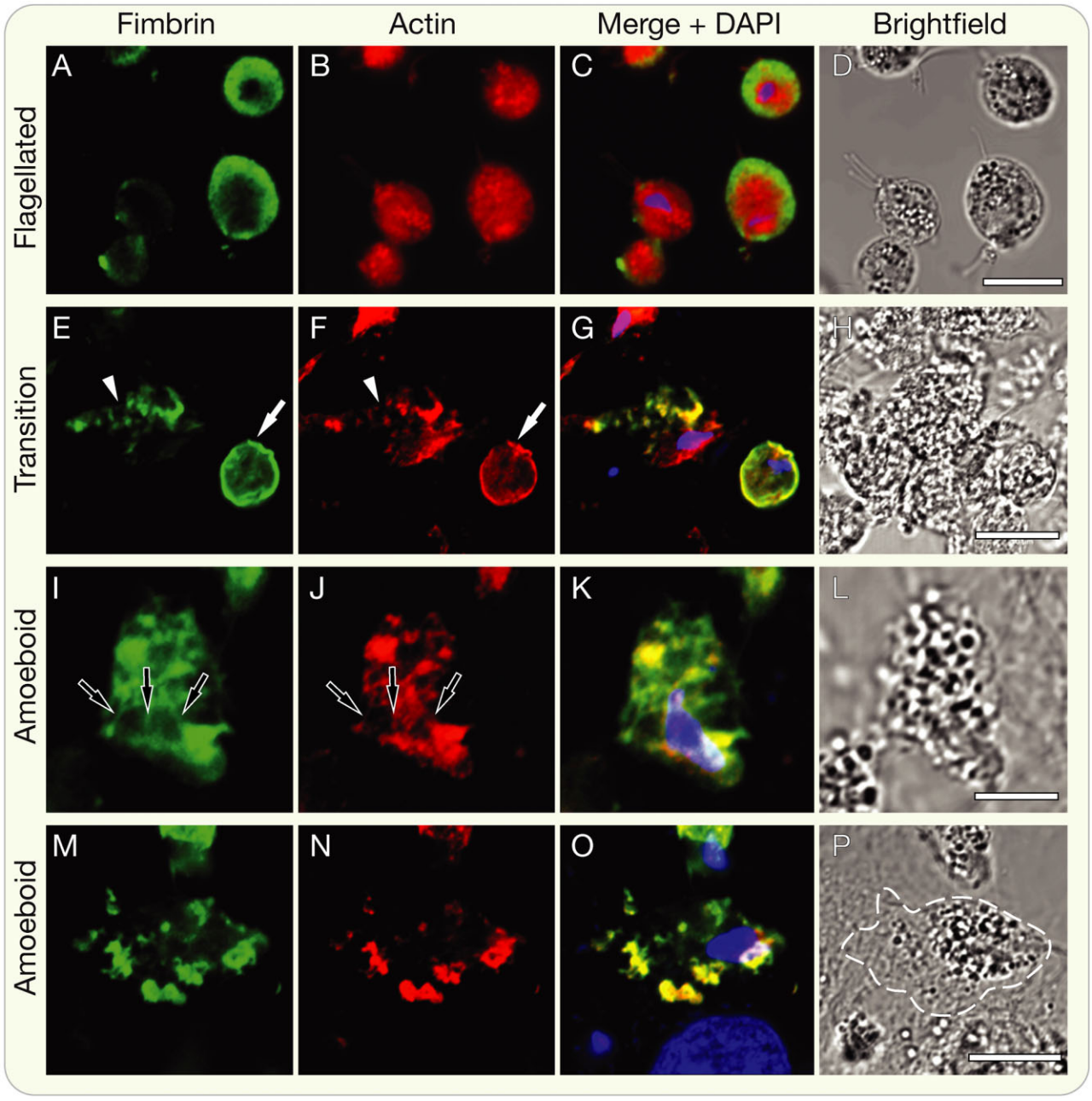

Fig. 5. Immunolocalization comparison of *Tv*Fim1 in free-swimming and adherent-amoeboid cells. In flagellated motile cells fimbrin localizes to the periphery of the cells in a gradient-like manner with no obvious actin colocalization (A–D). In cells exposed to vaginal epithelial cells (E–P) fimbrin colocalizes with actin, associates with structures reminiscent of actin cables (arrows in I and J) and shows peripheral clustering together with actin (M–O). In (E–G) a still pyriform cell can be seen, in which actin and fimbrin already localize in a sharp ring at the cells periphery (arrow) and next to a fully adherent cell with a very different labelling pattern (arrow head). The dashed line in (P) outlines the parasite based on the fluorescent channels of fimbrin and actin. Scale: 10 μm.

phagocytic vesicle, but at the same time highlights a range of other subcellular structures, including some punctuate staining and again fibrous patterns (Fig. 7).

Discussion

Through the characterization of the fimbrin protein family and live cell imaging of *T. vaginalis* we provide detailed evidence that the parasite's amoeboid morphogenesis during infection is accompanied by a rapid reorganization of the actin cytoskeleton. The flagellate to amoeboid transformation occurs several times faster in *T. vaginalis* than in *N. gruberi* (Arroyo *et al*., 1993; Fritz-Laylin *et al*., 2010a). We suggest that this might be attributable to the prey-induced activation of 'sleeping' components, such as

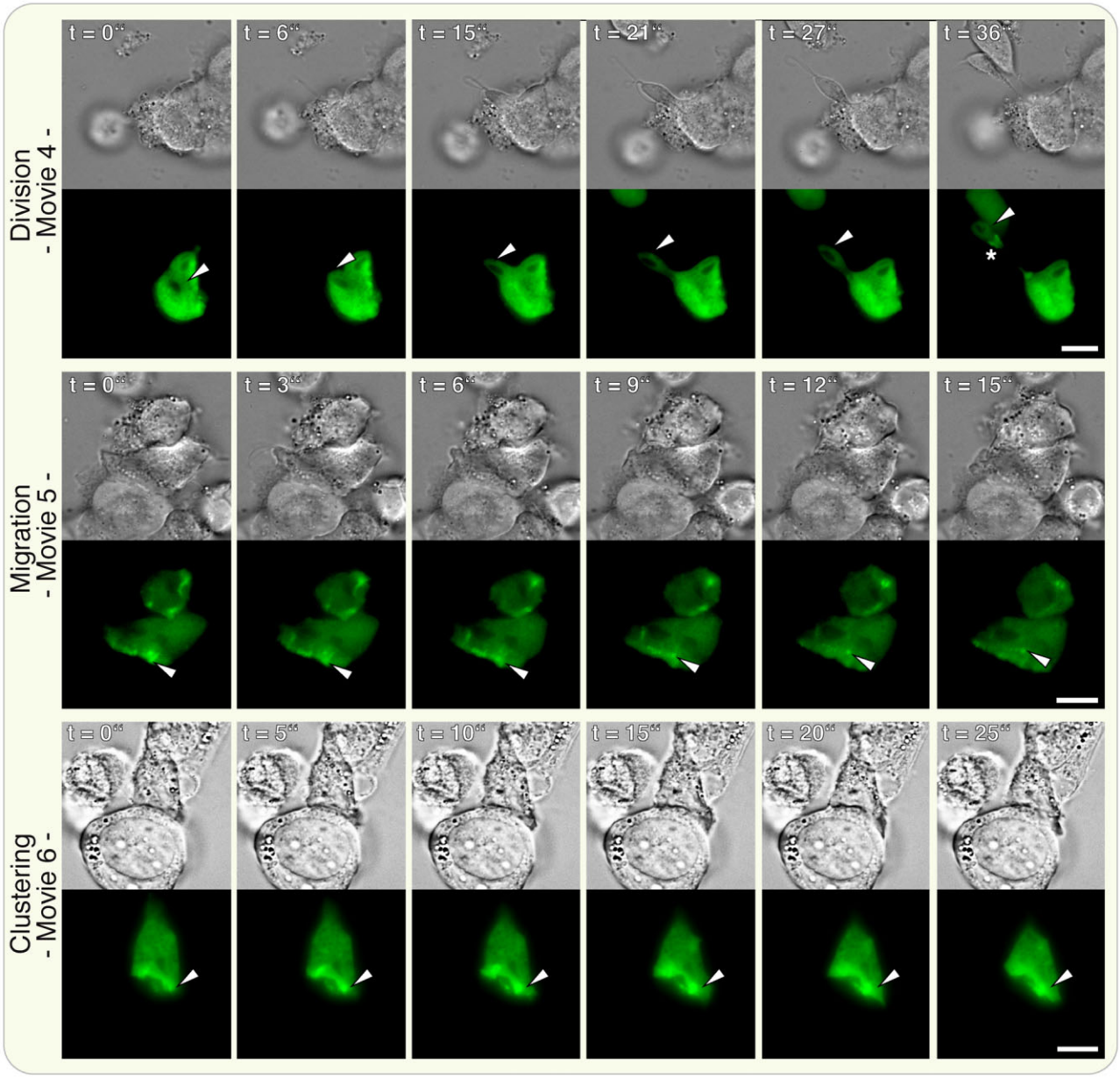

Fig. 6. Live imaging of *Tv*Fim1::GFP on host tissue. In the top panel a daughter cell can be seen to bud from the mother cell. *Tv*Fim1::GFP concentrates around a contractile ring-like structure (indicated by an asterisk) towards the basal end of the daughter cell during separation. During amoeboid migration across host tissue individual waves of *Tv*Fim1::GFP were clearly visible (wave indicated by arrow heads in the central panel). Clustering of *Tv*Fim1::GFP was predominantly found to occur around the initial host contact sites (indicated by arrow heads in the bottom panel). Images were taken 15 min (for clustering) and 70 min (for division and migration) after inoculation of host tissue with *T. vaginalis* respectively. Scale: 10 μm.

the *T. vaginalis* fimbrin protein *Tv*Fim1. Accordingly, the abundance and gradient-like localization of the actin-bundling protein below the plasma membrane in the flagellate form (Fig. 5A–C) appears to be a prearrangement that keeps the free-swimming parasite primed for actin cytoskeleton mediated phenotypic plasticity upon contact with host tissue. With the molecular machinery required already in place, only the final signal at the end of the activation cascade (such as calcium depletion or an altered phosphorylation state of the protein; see below) is required to trigger morphogenesis. This would explain why no significant upregulation of *Tv*Fim1 during infection is detected, when compared with a copy of the 40S ribosomal protein S5. By contrast, upregulation of alpha-actinin using semi-quantitative PCR has been reported to occur during infection (Noël *et al.*, 2010), whereby expression

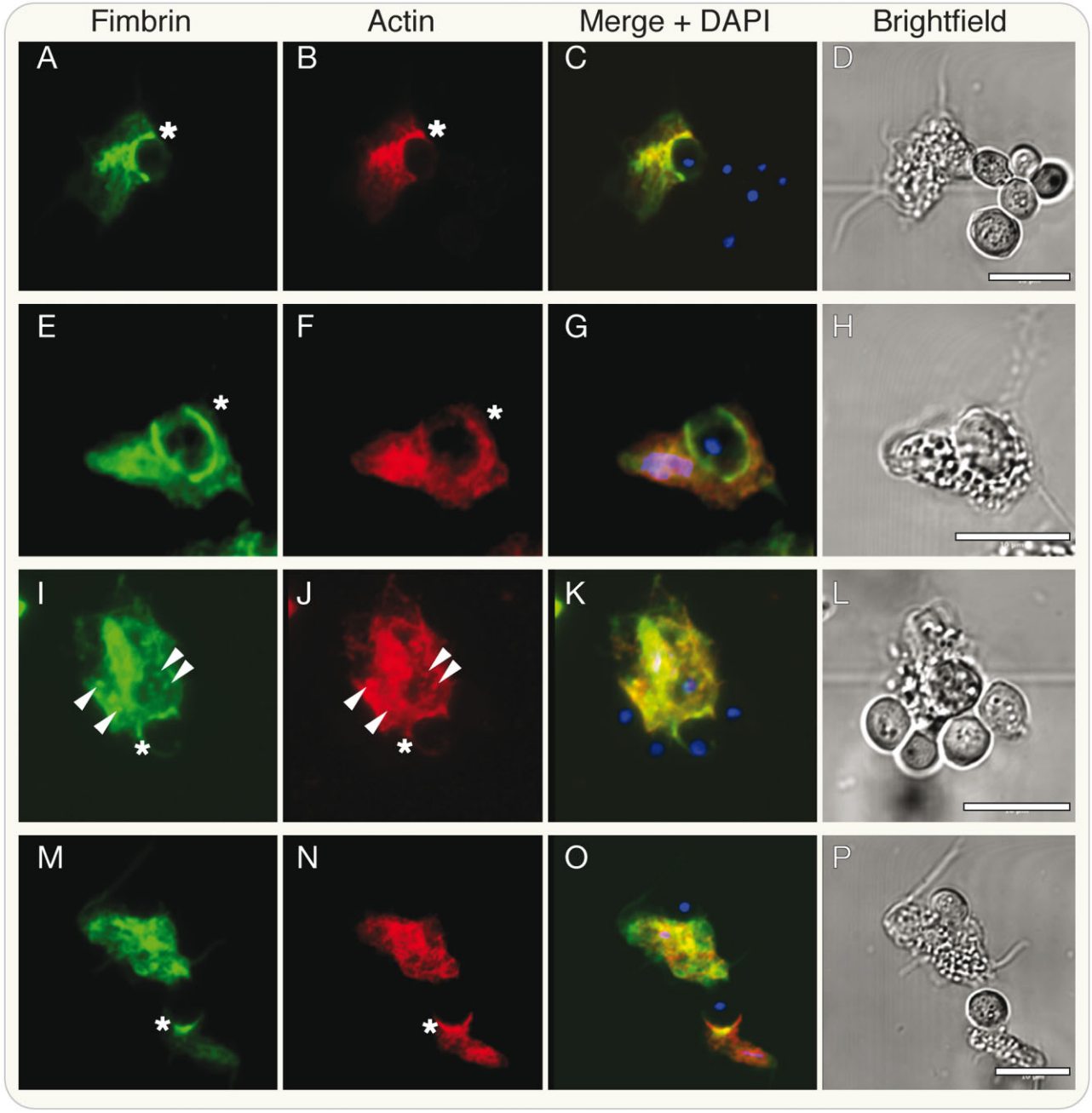

Fig. 7. Fimbrin and actin localization during phagocytosis. During phagocytosis of yeast cells actin and its bundling protein fimbrin colocalize and predominantly cluster around bordering phagocytic vesicles (asterisks). Other structures, in parts similar to those observed upon contact with host tissue, are also apparent, including smaller vesicular particles (arrow heads). Scale: 10 μm.

analysis in *Trichomonas* is in general impaired by the many gene duplicates present.

The majority of known core components of actin regulation are encoded by *Trichomonas* (Fig. 1), and some gene families have been significantly expanded in the course of genome duplication (Carlton *et al.*, 2007). Paralogous copies of many genes are present and simultaneously expressed. Proteins of the *Trichomonas* actin family are encoded in 29 copies and expression evidence exists for 24 of them at TrichDB. Only two genes encode proteins of the actin-bundling fimbrin family (TVAG_351310 and TVAG_116370) and the second, *Tv*Fim2, appears to be a pseudogene, a 5′ truncated paralogous copy of *Tv*Fim1. During or after gene duplication, *Tv*Fim2 lost the N-terminal EF-hand – the characteristic and regulatory module of fimbrin proteins – and with

it its function. We could neither detect expression of *Tv*Fim2 on RNA level through RT-PCR, supporting the lack of expression evidence on TrichDB, nor on protein level through Western blot analysis using our fimbrin antibody. The epitope of *Tv*Fim1 differs from that of *Tv*Fim2 by only one amino acid at position 185, which suggests the antibody should recognize both proteins. However, only one band of approximately 68 kDa and none of 50 kDa was detected (Fig. S3), corresponding to the predicted sizes of *Tv*Fim1 and *Tv*Fim2 respectively.

*Tv*Fim1 increases the polymerization rate of free *Acanthamoeba* actin, albeit weakly, and served as a potent filament cross-linker, bundling rabbit F-actin in a parallel and antiparallel manner (Fig. 4). Generally, fimbrin is not considered to be a canonical actin nucleator, such as formin or the ARP complex (Butler and Cooper, 2009). Our results are not yet able to determine the exact actin polymerization potency of *Tv*Fim1; however, we can exclude 'false positive polymerization' observed through scattering due to the settings in the pyrene assays. Experiments with purified *Trichomonas* actin are currently hindered, because it does not express well in any system tested. How, specifically, fimbrin increases actin polymerization is unknown for any model system, but independent experiments on homologues from yeast and *Arabidopsis* suggest that fimbrin might lower the necessary critical concentration for actin to polymerize (Cheng *et al*., 1999; Kovar *et al*., 2000). Intriguingly, only the polymerization of *Acanthamoeba* G-actin was significantly increased, but not of rabbit G-actin, although rabbit F-actin was clearly bundled by *Tv*Fim1. Amino acid residues that have been implicated in the interaction with actin are as well conserved in *Trichomonas* as in other eukaryotes (Fig. S1). Furthermore, the predicted tertiary structure of *Tv*Fim1 is almost identical to that of yeast (Fig. 3), and thereby fails to offer obvious clues as to the structural basis of the differential behaviour of *Tv*Fim1 to the different actins investigated here. However, our results provide further indirect evidence that fimbrin might be a weak nucleator, too, as the polymerization increase observed was not just due to a side-effect of the bundling of filamentous actin.

Hence, *T. vaginalis* expresses only one protein of the fimbrin family that, as shown here, fulfils all functions attributed to the fimbrin family and relocates during morphogenesis and phagocytosis. A knockout or knockdown of *Tv*Fim1 to underpin its importance during infection was at this point not successful. Knockouts could not be established – which only twice has been successful for *T. vaginalis* and only once reported to reveal a noticeable phenotype (Land *et al*., 2004; Pereira-Brás *et al*., 2013) – and expressing *Tv*Fim1 antisense RNA did not lead to a decrease of *Tv*Fim1 transcript (Fig. S7). Yet, modifications of fimbrin seemed to influence the transfected cells: (i) the HA-tagged line duplicated with only about half the speed, (ii) in a HaloTag line we could not detect any protein, albeit the construct was identified on RNA level (Fig. S6), suggesting either transcriptional inhibition or immediate post-translational degradation, (iii) the HA-tagged copy was also observed to show a degradation product not observed for the endogenous copy (Fig. S3B). In summary, fimbrin seems to fulfil pleiotropic roles, as indicated by its colocalization with actin during adherence to and migration across host cells and during phagocytosis of yeast, and a knockout or knockdown appears to influence the parasites viability.

The behaviour of *Tv*Fim1 during infection suggests the protein to be predominantly active during the amoeboid stage and most likely during phase transition from flagellate to the amoeboid. Clustering, specific aggregation and more defined localization of the protein were only observed in the adherent-amoeboid form of *Trichomonas* (Figs 5, 6 and S4) or during phagocytosis (Fig. 7). The signals that trigger morphogenesis and surface attachment are unknown, but *Tv*Fim1/actin re-localization and *Tv*Fim1-dependent actin polymerization provide new tools towards their investigation. *Trichomonas* can spontaneously adhere to glass and plastic surfaces and the amount of adherent cells increases when the surfaces are coated with fibronectin (Brugerolle *et al*., 1996). Only on VECs however have we observed that the vast majority of parasite cells undergo transition from a motile to an adherent stage over time. This suggests multiple signals and a complex cascade involving the correct recognition of host tissue. This is further supported by the fact that the parasite is also able to completely engulf and phagocytose other eukaryotes such as yeast – a process also involving a co-ordinated, but different re-localization of actin and fimbrin (Fig. 7). Phagocytosis must hence require a different downstream behaviour after prey recognition in comparison to adhering to VECs, and further unknown regulatory units orchestrating the different processes. Whether the activation of *Tv*Fim1 requires the EF-hand to not be bound to Ca^{++} (Namba *et al*., 1992; Prassler *et al*., 1997), or whether it is regulated through the phosphorylation of certain serine residues as shown for the human L-plastin (Shinomiya, 2012), remains to be investigated. *Tv*Fim1 has about 20 potential phosphorylation sites as predicted by NetPhos alone.

However, the different patterns of actin and fimbrin localization within the parasite during different morphological shifts reflect the complexity of actin and fimbrin dynamics in *Trichomonas*. In the amoeboid form actin and fimbrin colocalize in patches opposing the trailing end of the amoeba (Fig. 5M–O, Fig. 6, Fig. S4A–C), and with fibrous structures similar to those previously observed (Bricheux *et al*., 2000). The latter could represent actin

cable-like structures. These were also observed during phagocytosis of yeast to a minor degree, albeit here the clustering around the phagocytic vacuole was the predominant structure (Fig. 7). The punctate localization of fimbrin observed during phagocytosis (Fig. 7I–K) might represent endocytic vesicles that are known to associate with fimbrin-bundled actin filaments in mammals and yeast (Hagiwara *et al*., 2011; Skau *et al*., 2011). This would then furthermore suggest an interaction of *Tv*Fim1 with proteins of the Rab family, as observed for the mammalian Rab5 and fimbrin during endocytosis (Hagiwara *et al*., 2011).

The bundling of actin through fimbrin furthermore reflects only a fraction of the proteins likely associated with infection- and phagocytosis-related actin remodelling. Coronin has been localized to 'various dynamic subcortical zones' of the parasite, too, and suggested to play an important role during morphogenesis (Bricheux *et al*., 2000). In other eukaryotic systems actin-regulating proteins are known to together orchestrate a variety of processes, in particular those associated with motion (Golsteyn *et al*., 1997; Eichinger *et al*., 1999; dos Remedios *et al*., 2003; Xue *et al*., 2010). As mentioned earlier, the majority of these proteins are encoded by *T. vaginalis* (Fig. 1). One must predict that only their concerted effort allows the different responses observed upon contact with host tissue and yeast cells (Figs 5/6 and 7 respectively), and the elaborate patterns of motion revealed, which include swift migration across host tissue and a sweeping of the substrate through the constricted apical tip of the parasite (Movies S4–S10). The latter also supports previous findings, which suggested a flagella-localized tetraspanin (*Tv*TSP6) to serve sensory reception (de Miguel *et al*., 2012). *T. vaginalis* might therefore offer an alternative system to study the actin dynamics of a pathogenic protist.

In summary our results demonstrate that fimbrin likely assists actin bundling across a multitude of different processes and it appears that many of these functions are conserved among a diverse range of evolutionary distant eukaryotes. In the parasite *T. vaginalis* one of the primary function of the early actin-based – and fimbrin accompanied – morphogenesis includes phenotypic plasticity during host cell attachment: the increase of surface interactions with VECs to scavenge substrate while gliding across host tissue. Another function could include the feeding on, and defence against, other microorganisms of the vaginal flora the parasite likely encounters during infection. Our results confirm the actin machinery to accompany phagocytosis and the parasite has been shown to phagocytose a broad range of prokaryotic and eukaryotic cells (Street *et al*., 1984; Benchimol and de Souza, 1995; Rendon-Maldonado *et al*., 1998; Pereira-Neves and Benchimol, 2007). These observations shift the way we view parasite–host tissue interaction and offer a system and molecular proxy to study cytoskeletal actin dynamics in a protozoan parasite during infection-associated phenotypic morphogenesis.

Experimental procedures

Cultures

Trichomonas vaginalis strains T016, FMV1 and T1 were cultivated in tryptone–yeast extract maltose medium {2.22% (w/v) tryptose, 1.11% (w/v) yeast extract, 15 mM maltose, 9.16 mM L-cysteine, 1.25 mM L(+)ascorbic acid, 0.77 mM KH_2PO_4, 3.86 mM K_2HPO_4, 10% (v/v) horse serum, 0.71% (v/v) iron solution [= 1% (w/v) $Fe(NH_4)_2(SO_4) \times 6H_2O$, 0.1% (w/v) 5-sulfosalicylacid]} at 37°C and 5% CO_2 in a Galaxy 48R (Eppendorf, Germany). Immortalized VECs (VECs MS-74) were cultivated in 45% DMEM (Invitrogen, #31885), 45% Keratinocyte-SFM (Invitrogen, #37010022) and 10% fetal calf serum (FCS) in standard cell culture flasks (75 cm^2) and at the same conditions as *T. vaginalis*. At high confluency, cells were washed twice with Dulbecco's PBS (PAA, #H15-001), digested with trypsin (Invitrogen, #25300-054) for 5 min, before inactivation with FCS. Cells were then pelletized and resuspended in fresh media and split 1:10 into new flasks and medium. To prevent bacterial contamination a penicillin/streptomycin mix was added to a final concentration of 100 $\mu g\ ml^{-1}$ to both media.

Database screening and structure prediction

We compiled a list of 77 actin and tubulin associated genes, mainly from *Homo sapiens* (Table S1). These query sequences were matched against the complete genomes of 25 eukaryotes representing the different eukaryotic phyla (Table S2). The proteomes were obtained from RefSeq (Pruitt *et al*., 2007) except *Bigelowiella natans* (http://genome.jgi-psf.org/Bigna1/), *Cyanidioschyzon merolae* (Matsuzaki *et al*., 2004) and *Cyanophora paradoxa* (Price *et al*., 2012), which were downloaded from the corresponding genome project homepages. For five species without complete genomic sequences, ESTs were obtained downloaded from dbEST (Boguski *et al*., 1993; see also Table S2). Clusters of homologous proteins were reconstructed from a total of 453 696 proteins encoded within the eukaryotic chromosomes. A BLAST (Altschul *et al*., 1997) search analysis yielded 1497 best BLAST hits. All protein pairs were globally aligned using Needleman–Wunsch algorithm with needle program (Rice *et al*., 2000). A total of 12 758 protein pairs having global amino acids identities $\geq$ 20% were clustered into protein families using MCL algorithm (Enright *et al*., 2002) with the default parameters. The query proteins within each cluster were BLASTed against ESTs from *Alexandrium tamarense*, *Oxyrrhis marina*, *Porphyra yezoensis*, *Reclinomonas americana* and *Physarum polycephalum*, and matching ESTs were translated to amino acid sequences and added to the clusters based on the highest similarity. Clusters were further refined by splitting of paralogous clusters, merging of orthologous clusters, removing of single gene clusters and obvious paralogous sequences from a cluster, based on protein annotations and examination of phylogenetic trees reconstructed using PHYML (Guindon *et al*., 2010). This procedure yielded 62 protein families with a total of 891 genes.

The tertiary structure of *Tv*Fim1 (without the EF-hand) was generated on the basis of the known crystal structure of the *Schizosaccharomyces pombe* fimbrin PDB accession 1RT8 (Klein *et al*., 2004), using the MODELLER software (Eswar *et al*., 2006). A local alignment of *Tv*Fim1 to 1RT8 in MODELLER revealed an identity of 46% over an alignment length of 456 amino acids, representing the highest level of sequence similarity in the PDB database (http://www.rcsb.org/pdb/). In order to model the actin/ABD2 complex structure we used the structure of the F-actin-fimbrin/plastin ABD2 complex of *Homo sapiens* PDB accession 3BYH (Galkin *et al*., 2008) together with *Tv*Fim1 and an abundantly expressed actin of *T. vaginalis* (TVAG_337240).

Gene cloning and heterologous overexpression of Tv*Fim1*

*Tv*Fim1 gene sequence was amplified by *Tv*Fim1_NdeI_FOR (5′-CTGACGCATATGGCTGTAAACGCTGCG-3′) and *Tv*Fim1_BamHI_REV (5′-GACGTGGATCCTTGATCCATGGCCATAAGAGA-3′) using a proof-reading polymerase and ligated into expression vector pTagvag2 for IFAs, p*Tv*GFP [based on pTagvag2 with a *Trichomonas* codon-optimized green fluorescent protein (GFP)-tag replacing the HA] for live cell imaging of FMV1 and pETEV21a for overexpression respectively, and verified by sequencing. Thirty micrograms of the plasmid DNA was used for transfection of 2.5×10^8 *T. vaginalis* cells using standard electroporation (Delgadillo *et al*., 1997). After 4 h of incubation neomycine (G418) was added to a final concentration of 100 μg ml^{-1} for selection. For heterologous overexpression *E. coli* C41(DE3) was used and transformed with pETEV21a including the gene of interest. Briefly, 1 l of culture was incubated on an orbital shaker at 37°C until an optical density of OD_{600} 0.4–0.6 was reached. Overexpression was induced with 1 mM isopropyl-β-D-thiogalactopyranoside (IPTG) followed by a 4 h incubation at 37°C. Cells were pelletized, washed once with phosphate-buffered saline (PBS) and again pelletized. Cells were lysed by plotting and subsequent disruption using the OneShot disruptor (Constant Systems Limited). HIS-tagged protein was isolated using a HISTrap column (HisTrap HP 5 ml, GE Healthcare) and standard fast protein liquid chromatography on an Äkta P-920 (GE Healthcare).

Quantitative real-time PCR

All experiments were carried out using a StepOnePlus and Power SYBR Green master mix (Applied Biosystems). *T. vaginalis* RNA was isolated from biological triplets using TRIzol (Invitrogen) from the motile-flagellated and three adherent-amoeboid stages at 5, 20 and 60 min after fibronectin-induced morphogenesis (fibronectin from human plasma; Sigma F0895). RNA was transcribed into cDNA with iScript cDNA Synthesis Kit (Bio-Rad) and used as a template for real-time quantitative PCR. Primers used were: Fimbrin: *Tv*Fim1_qFOR: 5′-ACAACCTTTACGACGGCATC-3′ and *Tv*Fim1_qREV: 5′-GCTTTGTCTTGTTGGCCTTC-3′, 40S ribosomal protein S5: 40SRibo_qFOR: 5′-GCATTGATCAGGCTCTCTCC-3′, 40SRibo_qREV: 5′-ATGCGCTCAAGTTCGTCTTT-3′. For absolute quantification, a linear relationship of Ct and log (DNA weight) was plotted for the target transcripts and used to infer its corresponding amount. As the target gene sequence was known, the copy numbers implied in the quantity may be calculated by the molecular weight of the sequence, which led to the estimate of the transcript number in the unknown sample (Lu *et al*., 2012).

Western blotting and immunofluorescence

Protein samples were separated through standard SDS-PAGE and blotted onto nitrocellulose membrane. Membranes were blocked in 5% milk powder in Tris-buffered saline pH 7 (blocking buffer) for 30 min. Blots were incubated with the primary antibody at a dilution of 1:1000 or 1:5000 in blocking buffer either overnight at 4°C or for 1 h at room temperature (RT) and then washed 3× with TBS-T (TBS + 0.1% Tween 20), followed by the incubation with the secondary antibody (1:2000 or 1:10 000) and identical subsequent washes. Detection of the chemiluminescence signal was performed through the SuperSignal West Pico Chemiluminescent Substrate Kit (Thermo Scientific) according to the manufacturer's protocol.

For immunofluorescent labelling all wells of CultureSlides (BD Falcon, #354114) were loaded with about 1.5×10^5 VECs 48 h prior to fixation and incubated at 37°C and 5% CO_2. Medium was discarded, followed by the inoculation with 1.5×10^6 *T. vaginalis* cells for a minimum of 15 min at 37°C and 5% CO_2. Supernatant was discarded, adhesive cells washed gently with PBS and fixed and permeabilized with a solution containing 4% PFA and 0.1% Triton X-100 in PBS for 15 min at RT. After discarding the solution, cells were blocked (1% BSA, 0.25% Gelatine, 0.05% Tween 20 in PBS) for 30 min at RT. Slides were incubated with the primary antibody (1:50 to 1:500 in blocking buffer) for 1 h at RT, supernatant discarded and slides washed at least twice with PBS before incubation with the secondary antibody at 1:2500 to 1:5000 for 1 h at RT in the dark. Cells were then mounted in Fluoroshield with DAPI (Sigma #F6057). Samples were stored at 4°C, dark, until imaging using a Zeiss LSM 710 confocal microscope. Primary antibodies: polyclonal peptide antibody *Tv*Fim produced in rat (Eurogentec) against amino acid sequence CRK-FVGPREIVKGNQR, monoclonal HA-antibody (Sigma #H9658), monoclonal actin-antibody (Sigma #A4700) and mouse anti-GFP (Invitrogen #332600). Secondary antibodies: AlexaFluor488-anti-mouse IgG (Invitrogen #A11001), AlexaFluor594-anti-rat IgG (Invitrogen #A11007), ImmunoPure Goat Anti-Mouse IgG and Anti-Rat IgG (Pierce #31430 and #31470 respectively). Additional actin staining through TexasRed-X phalloidin (Invitrogen #T7471).

Yeast powder (RUF Lebensmittelwerk KG, Quakenbrück, Germany) was resuspended in sterile water (37°C) and washed three times with 0.1 M PBS. The cells were then resuspended in TYM-medium without serum at a concentration of 5×10^7 cells ml^{-1} and immediately used for the phagocytosis assay. *T. vaginalis* and yeast were mixed with a ratio of 1:50 in TYM without serum and incubated on CultureSlides (BD Falcon, #354114) for 1 h at 37°C and at 5% CO_2. Immunofluorescent labelling and microscopy was identical to the steps described above.

Live imaging

For live imaging μ-Slide VI 0.4 (Ibidi, #80606) was used. All six slide chambers were pre-loaded with 9×10^3 VECs, 48 h prior to infection and incubated at 37°C and 5% CO_2. Medium was

discarded, followed by the inoculation with 9×10^4 *T. vaginalis* cells and immediate microscopy, using a Zeiss AxioObserver.Z1 microscope with AxioCam MRm (real-time) and AxioCam ICC1 (time-lapse) at 37°C and 5% CO_2.

Actin polymerization assays

TIRF microscopy was carried out using the Zeiss Laser TIRF3 microscope at the Summer School on Actin Dynamics in Regensburg (DFG program SPP 1464). Actin polymerization was performed using 1.5 μM rabbit muscle actin alone as a control and in the presence of 3 and 5 μM *Tv*Fim1 in FPLC elution buffer (50 mM Tris-HCl pH 7.5, 300 mM NaCl, 500 mM imidazole, 1 mM NaN_3). Protein mixtures were diluted in freshly prepared fluorescence buffer containing 10 mM imidazole-HCl (pH 7.8), 50 mM KCl, 1 mM $MgCl_2$, 100 mM dithiothreitol, 3 mg ml^{-1} glucose, 20 μg ml^{-1} catalase, 100 mg ml^{-1} glucose oxidase and 0.5% methylcellulose to induce actin polymerization. Actin polymerization was induced in a solution containing 1.5 μM actin monomers (7% labelled with Alexa 568) and 3 or 5 μM *Tv*Fim1 respectively. Actin polymerization assays were monitored using the microplate reader Infinite200 PRO (Tecan Group, Ltd) and a Nunclon 96 flat black well plate. G-actin mix [4 μM unlabelled *Acanthamoeba* actin, 5% pyrene-actin in G-buffer (2 mM Tris pH 8.0, 0.5 mM DTT, 0.2 mM ATP, 0.1 mM $CaCl_2$, 0.01% NaN_3)] was measured alone and including 4 μM of *Tv*Fim1 with the following parameters: excitation = 365 nm, emission = 410 nm, Z position = 17 000, gain = 135, read every 3 s for 30 min.

Acknowledgements

We thank G. Landan and S. Nelson-Sathi for help with MatLab, all supervisors of the Actin Summer School of 2011 at the Universitätsklinikum Regensburg (Germany), in particular Margot Quinlan (University of California, USA) for helpful discussions. We thank J. Alderete and M. Benchimol for sharing *T. vaginalis* strains. This work was funded by a DFG grant (GO 1825/3-1) and the support of the 'Stiftung zur Erforschung infektiös-immunologischer Erkrankungen' to S.B.G.

References

Addis, M.F., Rappelli, P., Delogu, G., Carta, F., Cappuccinelli, P., and Fiori, P.L. (1998) Cloning and molecular characterization of a cDNA clone coding for Trichomonas vaginalis alpha-actinin and intracellular localization of the protein. *Infect Immun* **66:** 4924–4931.

Altschul, S.F., Madden, T.L., Schäffer, A.A., Zhang, J., Zhang, Z., Miller, W., and Lipman, D.J. (1997) Gapped BLAST and PSI-BLAST: a new generation of protein database search programs. *Nucleic Acids Res* **25:** 3389–3402.

Arroyo, R., González Robles, A., Martínez Palomo, A., and Alderete, J. (1993) Signalling of *Trichomonas vaginalis* for amoeboid transformation and adhesin synthesis follows cytoadherence. *Mol Microbiol* **7:** 299–309.

Aurrecoechea, C., Brestelli, J., Brunk, B.P., Carlton, J.M., Dommer, J., Fischer, S., *et al*. (2009) GiardiaDB and TrichDB: integrated genomic resources for the eukaryotic protist pathogens *Giardia lamblia* and *Trichomonas vaginalis*. *Nucleic Acids Res* **37:** D526–D530.

Baum, J., Tonkin, C.J., Paul, A.S., Rug, M., Smith, B.J., Gould, S.B., *et al*. (2008) A Malaria parasite formin regulates actin polymerization and localizes to the parasite-erythrocyte moving junction during invasion. *Cell Host Microbe* **3:** 188–198.

Benchimol, M. (2004) Trichomonads under microscopy. *Microsc Microanal* **10:** 528–550.

Benchimol, M. (2008) The hydrogenosome as a drug target. *Curr Pharm Des* **14:** 872–881.

Benchimol, M., and de Souza, W. (1995) Carbohydrate involvement in the association of a prokaryotic cell with *Trichomonas vaginalis* and *Tritrichomonas foetus*. *Parasitol Res* **81:** 459–464.

Boguski, M.S., Lowe, T.M., and Tolstoshev, C.M. (1993) dbEST-database for 'expressed sequence tags. *Nat Genet* **4:** 332–333.

Bricheux, G., Coffe, G., Pradel, N., and Brugerolle, G. (1998) Evidence for an uncommon alpha-actinin protein in *Trichomonas vaginalis*. *Mol Biochem Parasitol* **95:** 241–249.

Bricheux, G., Coffe, G., Bayle, D., and Brugerolle, G. (2000) Characterization, cloning and immunolocalization of a coronin homologue in *Trichomonas vaginalis*. *Eur J Cell Biol* **79:** 413–422.

Brugerolle, G., Bricheux, G., and Coffe, G. (1996) Actin cytoskeleton demonstration in *Trichomonas vaginalis* and in other trichomonads. *Biol Cell* **88:** 29–36.

Butler, B., and Cooper, J.A. (2009) Distinct roles for the actin nucleators Arp2/3 and hDia1 during NK-mediated cytotoxicity. *Curr Biol* **19:** 1886–1896.

Carlton, J.M., Hirt, R.P., Silva, J.C., Delcher, A.L., Schatz, M., Zhao, Q., *et al*. (2007) Draft genome sequence of the sexually transmitted pathogen *Trichomonas vaginalis*. *Science* **315:** 207–212.

Cheng, D., Marner, J., and Rubenstein, P.A. (1999) Interaction *in vivo* and *in vitro* between the yeast fimbrin, SAC6P, and a polymerization-defective yeast actin (V266G and L267G). *J Biol Chem* **274:** 35873–35880.

Delgadillo, M.G., Liston, D.R., Niazi, K., and Johnson, P.J. (1997) Transient and selectable transformation of the parasitic protist *Trichomonas vaginalis*. *Proc Natl Acad Sci USA* **94:** 4716–4720.

Eichinger, L., Lee, S.S., and Schleicher, M. (1999) *Dictyostelium* as model system for studies of the actin cytoskeleton by molecular genetics. *Microsc Res Tech* **47:** 124–134.

Elmendorf, H.G., Hayes, R.D., Srivastava, S., and Johnson, P.J. (2010) New insights into the composition and function of the cytoskeleton in *Giardia lamblia* and *Trichomonas vaginalis*. In *Anaerobic Parasitic Protozoa: Genomics and Molecular Biology*. Clark, C.G., Johnson, P.J., and Adam, R.D. (eds). Norfolk: Caister Academic Press, pp. 119–156.

Enright, A.J., Van Dongen, S., and Ouzounis, C.A. (2002) An efficient algorithm for large-scale detection of protein families. *Nucleic Acids Res* **30:** 1575–1584.

Eswar, N., Webb, B., Marti-Renom, M.A., Madhusudhan, M.S., Eramian, D., Shen, M.Y., *et al*. (2006) Comparative protein structure modeling using Modeller. *Curr Protoc Bioinformatics* **5:** Unit 5.6.

Fritz-Laylin, L.K., Prochnik, S.E., Ginger, M.L., Dacks, J.B., Carpenter, M.L., Field, M.C., *et al*. (2010a) The genome of *Naegleria gruberi* illuminates early eukaryotic versatility. *Cell* **140:** 631–642.

Fritz-Laylin, L.K., Assaf, Z.J., Chen, S., and Cande, W.Z. (2010b) *Naegleria gruberi* de novo basal body assembly occurs via stepwise incorporation of conserved proteins. *Eukaryot Cell* **9:** 860–865.

Fukui, Y. (2002) Mechanistics of amoeboid locomotion: signal to forces. *Cell Biol Int* **26:** 933–944.

Fulton, C. (1993) *Naegleria* – a research partner for cell and developmental biology. *J Euk Microbiol* **40:** 520–532.

Galkin, V.E., Orlova, A., Cherepanova, O., Lebart, M.-C., and Egelman, E.H. (2008) High-resolution cryo-EM structure of the F-actin-fimbrin/plastin ABD2 complex. *Proc Natl Acad Sci USA* **105:** 1494–1498.

Gold, D., and Ofek, I. (1992) Adhesion of *Trichomonas vaginalis* to plastic surfaces: requirement for energy and serum constituents. *Parasitology* **105:** 55–62.

Golsteyn, R.M., Louvard, D., and Friederich, E. (1997) The role of actin binding proteins in epithelial morphogenesis: models based upon *Listeria* movement. *Biophysl Chem* **68:** 73–82.

Guindon, S., Dufayard, J.F., Lefort, V., Anisimova, M., Hordijk, W., and Gascuel, O. (2010) New algorithms and methods to estimate maximum-likelihood phylogenies: assessing the performance of PhyML 3.0. *Syst Biol* **59:** 307–321.

Hagiwara, M., Shinomiya, H., Kashihara, M., Kobayashi, K., Tadokoro, T., and Yamamoto, Y. (2011) Interaction of activated Rab5 with actin-bundling proteins, L- and T-plastin and its relevance to endocytic functions in mammalian cells. *Biochem Biophys Res Comm* **407:** 615–619.

Jansen, S., Collins, A., Yang, C., Rebowski, G., Svitkina, T., and Dominguez, R. (2011) Mechanism of actin filament bundling by fascin. *J Biol Chem* **286:** 30087–30096.

Klein, M.G., Shi, W., Ramagopal, U., Tseng, Y., Wirtz, D., Kovar, D.R., *et al*. (2004) Structure of the actin crosslinking core of fimbrin. *Structure* **12:** 999–1013.

Korenbaum, E., and Rivero, F. (2002) Calponin homology domains at a glance. *J Cell Sci* **115:** 3543–3545.

Kovar, D., Staiger, C., Weaver, E., and McCurdy, D. (2000) *At*Fim1 is an actin filament crosslinking protein from *Arabidopsis thaliana*. *Plant J* **24:** 625–636.

Kulda, J. (1999) Trichomonads, hydrogenosomes and drug resistance. *Int J Parasitol* **29:** 199–212.

Lal, K., Noël, C.J., Field, M.C., Goulding, D., and Hirt, R.P. (2006) Dramatic reorganisation of *Trichomonas* endomembranes during amoebal transformation: a possible role for G-proteins. *Mol Biochem Parasitol* **148:** 99–102.

Land, K.M., Delgadillo-Correa, M.G., Tachezy, J., Vanacova, S., Hsieh, C.L., Sutak, R., and Johnson, P.J. (2004) Targeted gene replacement of a ferredoxin gene in *Trichomonas vaginalis* does not lead to metronidazole resistance. *Mol Microbiol* **51:** 115–122.

Lu, Y., Xie, L., and Chen, J. (2012) A novel procedure for absolute real-time quantification of gene expression patterns. *Plant Methods* **8:** 9.

Martincová, E., Voleman, L., Najdrová, V., De Napoli, M., Eshar, S., Gualdron, M., *et al*. (2012) Live imaging of mitosomes and hydrogenosomes by HaloTag technology. *PLoS ONE* **7:** e36314.

Matsuzaki, M., Misumi, O., Shin, I.T., Maruyama, S., Takahara, M., Miyagishima, S.Y., *et al*. (2004) Genome sequence of the ultrasmall unicellular red alga *Cyanidioschyzon merolae* 10D. *Nature* **428:** 653–657.

de Miguel, N., Riestra, A., and Johnson, P.J. (2012) Reversible association of tetraspanin with *Trichomonas vaginalis* flagella upon adherence to host cells. *Cell Microbiol* **14:** 1797–1807.

Namba, Y., Ito, M., Zu, Y., Shigesada, K., and Maruyama, K. (1992) Human T cell L-plastin bundles actin filaments in a calcium-dependent manner. *J Biochem* **112:** 503–507.

Noël, C.J., Diaz, N., Sicheritz-Ponten, T., Safarikova, L., Tachezy, J., Tang, P., *et al*. (2010) *Trichomonas vaginalis* vast BspA-like gene family: evidence for functional diversity from structural organisation and transcriptomics. *BMC Genomics* **11:** 99.

Paredez, A.R., Assaf, Z.J., Sept, D., Timofejeva, L., Dawson, S.C., Wang, C.J.R., and Cande, W. (2011) An actin cytoskeleton with evolutionarily conserved functions in the absence of canonical actin-binding proteins. *Proc Natl Acad Sci USA* **108:** 6151–6156.

Pereira-Brás, X., Zimorski, V., Bolte, K., Maier, U.-G., Martin, W.F., and Gould, S.B. (2013) Knockout of the abundant *Trichomonas vaginalis* hydrogenosomal membrane protein Tvhmp23 increases hydrogenosome size but induces no compensatory up-regulation of paralogous copies. *FEBS Lett* (in press). doi: 10.1016/j.febslet.2013.03.001.

Pereira-Neves, A., and Benchimol, M. (2007) Phagocytosis by Trichomonas vaginalis: new insights. *Biol Cell* **99:** 87–101.

Pereira-Neves, A., and Benchimol, M. (2009) *Tritrichomonas foetus*: budding from multinucleated pseudocysts. *Protist* **160:** 536–551.

Petrin, D., Delgaty, K., Bhatt, R., and Garber, G. (1998) Clinical and microbiological aspects of *Trichomonas vaginalis*. *Clin Microbiol Rev* **11:** 300–317.

Prassler, J., Stocker, S., Marriott, G., Heidecker, M., Kellermann, J., and Gerisch, G. (1997) Interaction of a *Dictyostelium* member of the plastin/fimbrin family with actin filaments and actin-myosin complexes. *Mol Biol Cell* **8:** 83–95.

Price, D.C., Chan, C.X., Yoon, H.S., Yang, E.C., Qiu, H., Weber, A.P.M., *et al*. (2012) *Cyanophora paradoxa* genome elucidates origin of photosynthesis in algae and plants. *Science* **335:** 843–847.

Pruitt, K.D., Tatusova, T., and Maglott, D.R. (2007) NCBI reference sequences (RefSeq): a curated non-redundant sequence database of genomes, transcripts and proteins. *Nucleic Acids Res* **35:** D61–D65.

dos Remedios, C.G., Chhabra, D., Kekic, M., Dedova, I.V., Tsubakihara, M., Berry, D.A., and Nosworthy, N.J. (2003) Actin binding proteins: regulation of cytoskeletal microfilaments. *Physiol Rev* **83:** 433–473.

Rendon-Maldonado, J.G., Espinosa-Cantellano, M., Gonzalez-Robles, A., and Martinez-Palomo, A. (1998) *Trichomonas vaginalis*: *in vitro* phagocytosis of lactobacilli, vaginal epithelial cells, leukocytes, and erythrocytes. *Exp Parasitol* **89:** 241–250.

Rice, P., Longden, I., and Bleasby, A. (2000) EMBOSS: the European Molecular Biology Open Software Suite. *Trends Genet* **16:** 276–277.

Ryan, C.M., de Miguel, N., and Johnson, P.J. (2011) *Trichomonas vaginalis*: current understanding of host-parasite interactions. *Essays Biochem* **51:** 161–175.

Santos, J.M., Lebrun, M., Daher, W., Soldati, D., and Dubremetz, J.-F. (2009) Apicomplexan cytoskeleton and motors: key regulators in morphogenesis, cell division, transport and motility. *Int J Parasitol* **39:** 153–162.

Shinomiya, H. (2012) Plastin family of actin-bundling proteins: its functions in leukocytes, neurons, intestines, and cancer. *Int J Cell Biol* **2012:** 213492.

Skau, C.T., Courson, D.S., Bestul, A.J., Winkelman, J.D., Rock, R.S., Sirotkin, V., and Kovar, D.R. (2011) Actin filament bundling by fimbrin is important for endocytosis, cytokinesis, and polarization in fission yeast. *J Biol Chem* **286:** 26964–26977.

Stark, J.R., Judson, G., Alderete, J.F., Mundodi, V., Kucknoor, A.S., Giovannucci, E.L., *et al*. (2009) Prospective study of *Trichomonas vaginalis* infection and prostate cancer incidence and mortality: Physicians' Health Study. *J Natl Cancer Inst* **101:** 1406–1411.

Street, D.A., Wells, C., Taylor-Robinson, D., and Ackers, J.P. (1984) Interaction between *Trichomonas vaginalis* and other pathogenic micro-organisms of the human genital tract. *Br J Vener Dis* **60:** 31–38.

Upcroft, P., and Upcroft, J.A. (2001) Drug targets and mechanisms of resistance in the anaerobic protozoa. *Clin Microbiol Rev* **14:** 150–164.

Xue, F., Janzen, D.M., and Knecht, D.A. (2010) Contribution of filopodia to cell migration: a mechanical link between protrusion and contraction. *Int J Cell Biol* **2010:** 507821.

Yusof, A., and Kumar, S. (2011) Ultrastructural changes during asexual multiple reproduction in *Trichomonas vaginalis*. *Parasitol Res* **110:** 1823–1828.

Supporting information

Additional Supporting Information may be found in the online version of this article at the publisher's web-site:

Table S1. Sources of seed sequences used in Fig. S1. The '*' indicate genes that were removed during the procedure of finding clusters of homologues, because they either had no homologues or were too similar to other gene families part of the list.

Table S2. Source of databases used to search for actin and tubulin associated genes.

Table S3. Observed migration speeds of *Trichomonas vaginalis* T016 exposed to the vaginal epithelial cell line MS74.

Fig. S1. Alignment of *Tv*Fim1 and its homologues from a range of eukaryotes is shown in (A). Known alpha-helical structures of the corresponding calponin homology domain (CH) are indicated above the alignment, whereas amino acids thought to be conserved residues for F-actin or suppressor residues are marked with a dot. Characterized actin binding sites are marked as a line below the alignment (based on Klein *et al*., 2004). (B) *Tv*Fim1 includes both, the EF-hand and four calponin homology domains (CH). *Tv*Fim2 is N-terminally truncated. For comparison, the human fimbrin protein (*Hs*Fim1, L-plastin) is only 16 amino acids longer and shares an overall sequence identity of 43% with *Tv*Fim1. The alignment was generated using the CLC Workbench and default settings and the following protein accessions: O.c., *Oryctolagus cuniculus* (XP_002720283.1); A.c., *Acanthamoeba castellanii* (ELR12888.1); S.p., *Schizosaccharomyces pombe* (NP596289.1); M.m., *Mus musculus* (AAH05459.1); H.s., *Homo sapiens* (AAB02845.1); G.g., *Gallus gallus* (P19179); D.m., *Drosophila melanogaster* (AAF48722.1); D.d., *Dictyostelium discoideum* (P54680); S.m., *Schistosoma mansoni* (AAC14025.1); G.p., *Gibberella pulicaris* (CAA10667.1); A.t., *Arabidopsis thaliana* (AAC39359.1).

Fig. S2. FPLC-purification of heterologously expressed *Tv*Fim1 from *Escherichia coli* strain C41. In (A) the FPLC run showing the loading, washing and elution phase with the elution peak of the HIS-tagged *Tv*Fim1 at 100 mM imidazol. (B) Coomassie-stained SDS-PAGE of 1: non-induced *E. coli* cell lysate; 2: induced *E. coli* cell lysate, 3: FPLC purified *Tv*Fim1 of 68 kDa (indicated by arrow). Marker (M) in kilodalton.

Fig. S3. Antibody controls.

A. Western blot of crude pre-immune (pIS) and immune rat sera (IS) from *Tv*Fim1 peptide immunization on protein extract from *Trichomonas vaginalis* and the *E. coli* strain expression recombinant *Tv*Fim1.

B. Western blot using purified *Tv*Fim1, HA-antibody and GFP-antibody on protein extract of the *T. vaginalis* strains expressing the corresponding constructs. Cropped bands of this blot were used for Fig. 2. Molecular marker (M) in kDa.

C. Immunofluorescence controls of the *T. vaginalis* strain T016 on fibronectin-coated slides using *Tv*Fim-pre-immune sera and anti-actin (Sigma). Scale bar: 10 μm.

D. shows the gradient-like colocalization of the HA-tagged *Tv*Fim1 with that of the endogenous copy towards the periphery of the cells. Scale bar: 2 μm.

Fig. S4. Additional *Tv*Fim1 distributions in *Trichomonas vaginalis* T016 cells. (A–D) *Tv*Fim1 concentrates at the protruding edge of a parasite, while gliding across host tissue, contour highlighted by a dashed line in (D). The protein furthermore associates with structures reminiscent of actin cables (E–H). Many parasites proliferate and become multinuclear (arrow heads) during infection (I–L). Arrow heads point to exemplary multi-nuclear cells. (M–R) Further localizations of fimbrin together with the hydrogenosomal marker enzyme ASCT (acetate : succinate CoA-transferase). Scale bar: 10 μm.

Fig. S5. Live cell imaging of *Trichomonas vaginalis* on human vaginal epithelial cells. Live imaging of the parasite exposed to human epithelial cells reveals *T. vaginalis* actively migrates across tissue, while they appear to use their flagella and apical tip as the guiding end. A clear trailing end and pseudopodia are also visible. While some rapidly divide on VECs, from what appears to be di-nuclear cells, others massively increase their size (juggernauting) and develop more than two nuclei and flagellar pockets before division. Areas of interest are marked with an asterisk in the first image of every series. For details please also refer to Movies S7–S10. Scale: 10 μm.

Fig. S6. A *Tv*Fim1::HaloTag fusion construct was generated using the identical primers as used for *Tv*Fim::HA construct (see Material & Methods of manuscript). The HaloTag plasmid (Martincová *et al*., 2012, *PLoS ONE* 7: e36314) was kindly provided by Pavel Dolezal (Charles University, Prague) and the product cloned into the plasmid through NdeI and BamHI and correct insertion verified through sequencing. RT-PCR and Western blot

analysis were carried out according to the methods described in the manuscripts main text. For live imaging of *Tv*Fim1 we fused the gene to the recently reported HaloTag (Martincová *et al*., 2012). We obtained several clones, three of which we analysed and shown above. (A) Reverse transcriptase PCR on RNA isolated from the transfected T016 cells and using specific primers, shows the fusion gene *Tv*Fim1::HaloTag is expressed in clones 2 and 3. (B) No fusion-protein is detected by Western blot analysis using an anti-haemagglutinin antibody (an HA-tag is included in the fusion protein generated by pHaloTag). This correlates with the lack of fluorescence during microscopic analysis of the clones.

Fig. S7. A. We tried to knockdown *Tv*Fim1 using anti-sense RNA as described previously by Ong *et al*. (2007, *JBC* 282: 6716–25). The anti-sense region was amplified from genomic DNA using the primers *Tv*Fim1-as_BamHI_F: 5′-GGTGGT GGATCCCGTATGAGCCTTCTCAAGAC-3′ and *Tv*Fim1-as_ NdeI_R: 5′-GGTGGTCATATGGCCGTCAGCGATGCCG-3′. After sequence verification the fragment was cloned into pTagvag2 for standard expression under the control of the SCS promoter. *T. vaginalis* was then transfected with 30 μg of plasmid DNA and selected through G418 (see 'Gene cloning' section).

B. RNA from recombinant and wild-type trichomonads was transcribed into cDNA and used as a template for real-time quantitative PCR using *Tv*Fim1 specific primers (see 'Quantitative PCR' section) and biological and technical triplicates. The expression level of *Tv*Fim1 in the wild type was used as the reference (100%) against *Tv*Fim1-as, which revealed no significant upregulation or downregulation of the gene.

Movie S1. Total internal reflection microscopy movie of actin self-assembly.

Movie S2. Total internal reflection microscopy movie of actin self-assembly in the presence of 3 μm *Tv*Fim1.

Movie S3. Total internal reflection microscopy movie of actin self-assembly in the presence of 5 μm *Tv*Fim1.

Movie S4. Live imaging of *Tv*Fim1::GFP. A daughter cell can be seen budding from a multinuclear mother cell that is attached to host tissue. Fimbrin::GFP is found to cluster around contractile ring-like structure of the daughter cell. One image was taken every 3 s and run at 7 frames per second.

Movie S5. Live imaging of *Tv*Fim1::GFP. During the migration of the parasite across tissue, waves of *Tv*Fim1::GFP can clearly be seen in close proximity to the migration front and moving away from it. One image was taken every 3 s and run at 7 frames per second.

Movie S6. Live imaging of *Tv*Fim1::GFP. Clustering of *Tv*Fim1::GFP was predominately observed to occur in areas of the parasite attaching to the vaginal epithelial cells. One image was taken every 5 s and run at 7 frames per second.

Movie S7. Time lapse movie of *T. vaginalis* on vaginal epithelial cells showing concerted movement and the parasite using the apical tip as the guiding end and for flagellar sensing. 40 min into infection and one image taken every second and run at 7 frames per second.

Movie S8. Time lapse movie of a *T. vaginalis* nicely showing the pseudopods and the trailing end of the parasite while gliding along host tissue 20 min after infection. One image was taken ever 0.2 s and run at 10 frames per second.

Movie S9. Time lapse movie of a *T. vaginalis* cell dividing on a vaginal epithelial cell just 5 min after infection. One image taken every second and run at 7 frames per second.

Movie S10. Time lapse movie of *T. vaginalis* on vaginal epithelial cells 70 min into infection, demonstrating some adherent cells to massively increase their overall cell mass, a process we refer to as juggernauting. One image taken every second and run at 28 frames per second.